

RESEARCH ARTICLE

The plasticity of the pyruvate dehydrogenase complex confers a labile structure that is associated with its catalytic activity

Jaehyoun Lee¹, Seunghee Oh¹, Saikat Bhattacharya¹, Ying Zhang¹, Laurence Florens¹, Michael P. Washburn^{1,2}, Jerry L. Workman^{1*}

1 Stowers Institute for Medical Research, Kansas City, Missouri, United States of America, **2** Department of Pathology and Laboratory Medicine, University of Kansas Medical Center, Kansas City, Kansas, United States of America

* jlw@stowers.org



OPEN ACCESS

Citation: Lee J, Oh S, Bhattacharya S, Zhang Y, Florens L, Washburn MP, et al. (2020) The plasticity of the pyruvate dehydrogenase complex confers a labile structure that is associated with its catalytic activity. *PLoS ONE* 15(12): e0243489. <https://doi.org/10.1371/journal.pone.0243489>

Editor: Oscar Millet, CIC bioGUNE, SPAIN

Received: August 10, 2020

Accepted: November 21, 2020

Published: December 28, 2020

Copyright: © 2020 Lee et al. This is an open access article distributed under the terms of the [Creative Commons Attribution License](https://creativecommons.org/licenses/by/4.0/), which permits unrestricted use, distribution, and reproduction in any medium, provided the original author and source are credited.

Data Availability Statement: All relevant data are within the manuscript and its [Supporting information](#) files.

Funding: Stowers Institute for Medical Research (<https://www.stowers.org>) and National Institutes of General Medical Sciences (<https://www.nigms.nih.gov>) grant R35GM118068 (J.L.W.). The content is solely the responsibility of the authors and does not necessarily represent the official views of the National Institutes of Health. The funders had no role in study design, data collection

Abstract

The pyruvate dehydrogenase complex (PDC) is a multienzyme complex that plays a key role in energy metabolism by converting pyruvate to acetyl-CoA. An increase of nuclear PDC has been shown to be correlated with an increase of histone acetylation that requires acetyl-CoA. PDC has been reported to form a ~ 10 MDa macromolecular machine that is proficient in performing sequential catalytic reactions via its three components. In this study, we show that the PDC displays size versatility in an ionic strength-dependent manner using size exclusion chromatography of yeast cell extracts. Biochemical analysis in combination with mass spectrometry indicates that yeast PDC (yPDC) is a salt-labile complex that dissociates into sub-megadalton individual components even under physiological ionic strength. Interestingly, we find that each oligomeric component of yPDC displays a larger size than previously believed. In addition, we show that the mammalian PDC also displays this uncommon characteristic of salt-lability, although it has a somewhat different profile compared to yeast. We show that the activity of yPDC is reduced in higher ionic strength. Our results indicate that the structure of PDC may not always maintain its ~ 10 MDa organization, but is rather variable. We propose that the flexible nature of PDC may allow modulation of its activity.

Introduction

The multienzyme pyruvate dehydrogenase complex (PDC) catalyzes the reaction that generates acetyl-CoA from pyruvate, the end-product of glucose breakdown. As such, the PDC plays a central role as a gatekeeper of energy and glucose homeostasis. Consistent with its important role in metabolism, low PDC activity arising from mutations of its components causes a PDC deficiency (PDCD) [1]. PDCD patients have a low survival rate and suffer from ataxia and neurodevelopmental delay. This arises from a failure to produce enough energy as the tricarboxylic acid (TCA) cycle, which links glycolysis to electron transport chain for ATP

and analysis, decision to publish, or preparation of the manuscript.

Competing interests: NO authors have competing interests.

synthesis, needs PDC to convert pyruvate into acetyl-CoA [1, 2]. Being a key enzyme in cellular metabolism, PDC is also considered a target for anticancer and antibacterial drugs [3, 4]. Furthermore, the level of nuclear PDC is correlated with that of histone acetylation as well as its recruitment to some promoters upon induction possibly for local acetyl-CoA production [5–8].

The central role of PDC in energy homeostasis necessitates a tight regulation of its activity. Short-term regulation (minutes to hours) occurs through the inhibitory phosphorylation of E1p α by pyruvate dehydrogenase kinases (PDKs) and phosphatases, while long-term regulation of PDC activity can be exerted at transcriptional levels within days to weeks [9, 10]. PDKs have been studied as potential drug targets as well because of their upregulation or activation in diseases such as diabetes and cancer [11, 12].

The catalysis of PDC is performed by three separate enzymes E1p (pyruvate dehydrogenase), E2p (dihydrolipoamide acetyltransferase), and E3 (dihydrolipoamide dehydrogenase), which are linked together efficiently into a large multienzyme complex, where the oligomeric E2p forms a structural core, to which multiple copies of the E1p, E3, and E3BP (E3 binding protein) are bound [13]. The E1p performs the rate-limiting oxidative decarboxylation of pyruvate via thiamine pyrophosphate (TPP) and transfers the acetyl-group to the lipoyl group of the E2p. Then the E2p transfers the acyl group to CoA while reducing its lipoyl domain, which is then oxidized by the E3 which transfers electrons to NAD⁺ via its cofactor FAD, resulting in the formation of NADH [14]. The formation of PDC not only allows substrate channeling between neighboring enzymes but also connects remote E1p and E3 within the complex by active-site coupling via flexible lipoyl domains of the E2p core [15–17].

Attempts to study the PDC has primarily used structure analysis methods such as analytical ultracentrifugation, Cryo-EM, crystallography, isothermal titration calorimetry, nuclear magnetic resonance spectroscopy, small-angle X-ray scattering and neutron scattering [18–24]. Interestingly, structural studies of the PDC have reported varying sizes of the complex [25–30]. Stoichiometry of the PDC subunits in the complex was shown to vary when prepared from *E. coli* [25, 26], and multiple sedimentation components of the bacterial PDC corresponding to different sizes were observed [27, 28]. Intriguingly, a study imaged pig heart PDC within sections of mitochondria where it displayed a size estimated to ~ 1–3 MDa in contrast to ~10 MDa estimated from sedimentation studies [30]. In this study, we used size exclusion chromatography (SEC) to examine the size of PDC in physiological condition. SEC is a well-established flow-assisted separation technique that can determine protein heterogeneity by separating native protein complexes in solution assisted by mass spectrometry [31]. Although SEC does not provide a detailed molecular information, it can determine hydrodynamic sizes of macromolecules from which oligomerization state(s) may be deduced. For a globular oligomeric complex like the PDC that may organize into multiform structures, SEC can give a good approximation of their sizes.

In this work, by using calibrated SEC using a gel filtration column, we demonstrate that the PDC displays size versatility in an ionic strength-dependent manner. Also, by performing immunoprecipitation followed by mass spectrometry along with SEC, we show that the individual PDC components can form sub-megadalton complexes in a physiological condition. We examine the biological implications of these findings by showing that the activity of PDC is reduced in high ionic strength. We propose that the versatile nature of PDC structure may allow modulation of its activity and translocation.

Materials and methods

Yeast strains and growth medium

Saccharomyces cerevisiae strains (BY4741) used in this study are listed in S1 Table in [S1 File](#). All single deletion mutants using KanMX4 marker were obtained from Open Biosystems library maintained by Stowers Institute Molecular Biology facility. The remaining strains were generated by targeted homologous recombination of PCR fragments with marker genes. The deletion or tagged strains were verified by PCR with primer sets specific for their deletion or tagging marker or coding regions. Growth and maintenance of *S. cerevisiae* strains were done in Yeast extract–Peptone–Dextrose medium (YPD, 2% glucose).

Yeast cell extractions and subcellular fractionation

Yeast cells were grown in YPD medium at 30°C to OD600 of 0.8. Cell pellet was washed and resuspended in 40 ml per 1,000 OD600 of SB buffer (1.4 M Sorbitol, 40 mM HEPES, pH 7.5, 0.5 mM MgCl₂, 10 mM β-mercaptoethanol) and spheroplasted with 2 mg/ml Zymolyase 20T (Amsbio LLC, 120491–1) at 23°C for 45 min. For whole cell extract, spheroplast was lysed with glass beads in TAP50 buffer (50 mM NaCl, 40 mM HEPES pH 7.5, 10% Glycerol, 0.1% Tween-20, 1 μg/ml pepstatin A, 2 μg/ml leupeptin, 1 mM PMSF) or EM150 (150 mM NaCl, 10 mM MOPS buffer pH 7.2, 1 mM EDTA, 1% Triton X-100, 1 μg/ml pepstatin A, 2 μg/ml leupeptin, 1 mM PMSF) at 4°C for 20 min. The whole cell extract was treated with 25 unit of Benzonase (Millipore Sigma, 70664) and 5 μg of heparin per 1,000 OD cells at 23°C for 15 min to remove nucleic acid contamination and then clarified by ultracentrifugation at 45,000 rpm for 90 min following a centrifugation at 20,000 g for 20 min. For the separation of high sedimentation rate fraction (HS) and low sedimentation rate fraction (LS) fractions, spheroplast was resuspended in 20 ml of homogenization buffer (10 mM Tris-HCl pH 7.4, 0.6 M sorbitol, 1 mM EDTA, 0.2% (w/v) BSA) and homogenized with 8 strokes of a revolving pestle at full speed per 1,000 OD600 cells. The homogenized spheroplast was centrifuged at 1,500 g for 5 min and the resulting pellet was collected as the LS fraction. The supernatant was further centrifuged at 3,000 g for 5 min then at 12,000 g for 15 min, when the final pellet was collected as the HS fraction. The HS fraction was washed with 6 ml of buffer C (0.25 M sucrose, 10 mM Tris pH 6.7, 0.15 mM MgCl₂) and D (0.25 M sucrose, 10 mM Tris pH 7.6, 10 mM EDTA), then finally resuspended in 1 ml of EM buffer (10 mM MOPS buffer pH 7.2, 1 mM EDTA, 1% Triton X-100, 1 μg/ml pepstatin A, 2 μg/ml leupeptin, 1 mM PMSF) with 0 mM (EM), 150 mM (EM150), or 350 mM NaCl (EM350) and homogenized with 50 strokes and incubated for 1 hr in ice with 5 units of Benzonase. The crude HS fraction was clarified by ultracentrifugation at 50,000 rpm for 30 min. The LS fraction was further clarified by washing the pellet with NP buffer (0.34 M sucrose, 20 mM Tris pH 7.5, 50 mM KCl, 5 mM MgCl₂) and homogenizing in H350 buffer (40 mM HEPES-KOH pH7.5, 10% glycerol, 350 mM KCl, 2 mM MgCl₂, 1 mM EDTA, 0.02% NP40), EM, or EM150 buffer with 25 strokes. The crude extract was incubated with 125 units of Benzonase on a roller for 1 hr in 4°C, then clarified by ultracentrifugation at 45,000 rpm for 90 min following a centrifugation at 20,000 g for 15 min.

FLAG purification

Clarified extract was incubated with anti-FLAG M2 agarose (Sigma-Aldrich, A2220) at 4°C for 4 hr and washed two times with its resuspending buffer and once with E100 buffer (25 mM HEPES-KOH pH7.5, 10% glycerol, 100 mM KCl, 2 mM MgCl₂, 1 mM EDTA with Roche cOmplete™, EDTA-free Protease Inhibitor Cocktail Tablets). The FLAG tagged proteins were eluted with E100 buffer containing 400 μg/ml 3xFLAG peptide.

Mammalian protein extraction and Halo purification

For Halo (HaloTag, Promega) purification, HEK293T cells at 40% confluency in a 100 mm plate were transfected with 10 μ g of plasmid containing ORF of PDHA1-HA-Halo or Halo-PDHA1 in 1X BBS (from 2XBBS (0.28 M NaCl, 0.05 M N,N-bis-(2-Hydroxyethyl)-2-aminoethanesulfonic acid, 1.5 mM Na₂HPO₄) with 125 mM CaCl₂. Cells were harvested by scraping in PBS following a PBS wash after 24 hr from transfection. For non-transfected cells, cells were harvested at 100% confluency. Cell pellet was resuspended in 1 ml of Hypotonic buffer (50 mM Tris-HCl pH 7.5, 0.1% NP-40) and centrifuged at 4000 rpm for 5 min. The resulting pellet was resuspended in 1 ml of lysis buffer (50 mM Tris-HCl pH 7.5, 1% Triton X-100, 0.1% Na-deoxycholate) with 0 mM, 150 mM, or 350 mM NaCl then clarified by centrifugation at 12,000 rpm for 30 min. The crude extract in the supernatant was treated with 125 units of benzonase for 20 min in 4°C, then clarified by centrifugation at 12,000 rpm for 10 min. The clarified extract was either directly loaded onto Superose 6 column following pre-clearing with 150 μ l of Sepharose CL-2B (GE Healthcare, 17-0140-01) or subjected to Halo purification by incubating with 100 μ l of HaloLink™ Resin (Promega, G1915) suspension overnight in 4°C on a rotator. The beads were washed 3 times then subjected for protein elution with 50 units of AcTEV protease (Invitrogen, 12575–015) in PBS buffer by 8 hr incubation in 4°C on a rotator.

Size-exclusion chromatography (SEC)

The size exclusion fractionation using Superose® 6 10/300 GL (GE17-5172-01) was performed as previously described [32] with minor modification. It was calibrated with standard proteins BSA (67 kDa), catalase (232 kDa), apoferritin (440 kDa), thyroglobulin (669 kDa, 1338 kDa) and Blue Dextran 2000 (2 MDa). Cell extracts following a pre-clearing with 150 μ l of Sepharose CL-2B or elution from FLAG of Halo purification was loaded onto a Superose 6 size-exclusion column (Amersham Bioscience) equilibrated with EM, EM50, or EM150 buffer for 0 mM, 50 mM, or 150 mM NaCl condition for yeast samples, PBS buffer or PBS minus NaCl and KCl for 150 mM or 0mM NaCl mammalian samples, or superose 6 buffer (350 mM NaCl, 40 mM HEPES pH 7.5, 5% glycerol, 0.1% Tween 20) for 350 mM NaCl condition. The 500 μ l fractions eluted from the column were analyzed by western blots and multidimensional protein identification technology as described in the results section.

Immunoblotting

SDS samples were run on 10% SDS-PAGE and transferred to 0.45 μ m Immobilon-P PVDF Membrane (Millipore Sigma, IPVH00010) and immunoblotted using anti-FLAG (Sigma-Aldrich, A8592) at 1:10,000 dilution in 5% non-fat milk, anti-HA (ThermoFisher Scientific, 26183-HRP) at 1:2,000 dilutions in 5% non-fat milk, anti-V5 (Abcam, ab9116) and anti-MTCO2 (Abcam, ab110271) at 1:1,000 dilutions in 5% non-fat milk, anti-Lamin A (Abcam, ab26300) and anti-E1 α (Abcam, ab110330) at 1:500 dilution in 5% BSA (Sigma-Aldrich, a9647), anti-E1 β (Abcam, ab155996), anti-E2 (Santa Cruz Biotechnology, sc-271534), anti-E3 (Santa Cruz Biotechnology, sc-365977), anti-BAF155 (Santa Cruz Biotechnology, sc-9746) at 1:2,000 dilution in 5% BSA, or anti-Brg1 (Abcam, ab110641) at 1:2,000 dilution in 5% BSA.

PDC activity assay

Iodonitrotetrazolium chloride (INT)-based colorimetric assay was performed base on previous publication [33] with minor modification. Briefly, yPDC was purified with FLAG M2 agarose from whole cell extract of *pkp2 Δ /Pdb1-5xFLAG* as described above. From 250 μ l elution of FLAG purification of Pdb1, 6 μ l was used for the assay. Assay was performed in 20 μ l reaction

with 50 mM potassium phosphate buffer pH 7.5, 2.5 mM β -Nicotinamide adenine dinucleotide (NAD⁺; Sigma Aldrich, N8410), 5 mM sodium pyruvate (Gibco, 11360070), 0.2 mM Thiamine pyrophosphate (TPP; Sigma Aldrich, C8754), 0.6 mM or 0.4 mM Iodonitrotetrazolium chloride (INT) (Sigma-Aldrich, I8377), 6.5 μ M Phenazine ethosulfate (PES; Sigma-Aldrich, P4544), 0.1 mM Coenzyme A trihydrate (VWR, IC10480950), 1 mg/ml BSA (Sigma-Aldrich, A9647), and 1 mM MgCl₂ with 50 mM, 100 mM or 350 mM NaCl. The amount of INT-formazan reduced by PES which was reduced by NADH from PDC activity was measured by the absorbance value at 490 nm by NanoDrop 2000 (ThermoFisher, ND-2000).

Proteomics analysis by multidimensional protein identification technology (MudPIT)

TCA-precipitated protein pellets were solubilized using Tris-HCl pH 8.5 and 8 M urea, followed by addition of TCEP (Tris(2-carboxyethyl)phosphine hydrochloride; Thermo Scientific, 20490) and chloroacetamide (CAM; Sigma-Aldrich, 22790) to final concentrations of 5 mM and 10 mM, respectively. Proteins were digested using Endoproteinase Lys-C at 1:100 w/w (Roche, 11058533103) at 37°C overnight. Digestion solutions were brought to a final concentration of 2 M urea and 2 mM CaCl₂ and a second digestion was performed overnight at 37°C using trypsin (Promega, v5280) at 1:100 w/w. The reactions were stopped using formic acid (5% final). Peptide samples were loaded on a split-triple-phase fused-silica micro-capillary column and placed in-line with a linear ion trap mass spectrometer (LTQ) (Thermo Scientific), coupled with a Quaternary Agilent 1100 Series HPLC system. A fully automated 10-step chromatography run (for a total of 20 hr) was carried out, as described in [34]. Each full MS scan (400–1600 m/z) was followed by five data-dependent MS/MS scans. The number of the micro scans was set to 1 both for MS and MS/MS. The dynamic exclusion settings used were as follows: repeat count 2; repeat duration 30 sec; exclusion list size 500 and exclusion duration 120 sec, while the minimum signal threshold was set to 100.

MS/MS peak files were extracted with RawDistiller [35] and searched using ProLuCID (v. 1.3.3) [36] against a database consisting of 5945 *S. cerevisiae* non-redundant proteins (NCBI, 2017-05-16), 193 usual contaminants (such as human keratins, IgGs, and proteolytic enzymes), and, to estimate false discovery rates (FDRs), 6138 randomized amino acid sequences derived from each non-redundant protein entry. The human dataset was searched against a database consisting of 36,628 *Homo sapiens* NR proteins (NCBI -released June 10, 2016), 193 usual contaminants, and randomized amino acid sequences derived from each NR protein entry. Mass tolerance for precursor and fragment ions was set at 800 ppm. ProLuCID searches were set up against a preprocessed database of tryptic peptides with K/R at both ends and with a differential modification of +16 Da on methionine residues. No maximum number of missed cleavages were specified. To account for alkylation by CAM, 57 Da were added statically to the cysteine residues.

Peptide/spectrum matches were sorted and selected using DTASelect/CONTRAST (v. 1.9) [37] in combination with an in-house software, swallow (v. 0.0.1, <https://github.com/tzw-wen/kite>), to filter spectra, peptides, and proteins at FDRs < 5%. Combining all runs, proteins had to be detected by at least 2 peptides or by 1 peptide with 2 independent spectra. To estimate relative protein levels, distributed normalized spectral abundance factors (dNSAF) were calculated for each detected protein, as described in [38]. The MS datasets for the human and yeast analyses may be obtained from the MassIVE repository with accessions MSV000085125 and MSV000085126, respectively (with password: JLE01146) and from the ProteomeXChange with accessions PXD018125 and PXD018126.

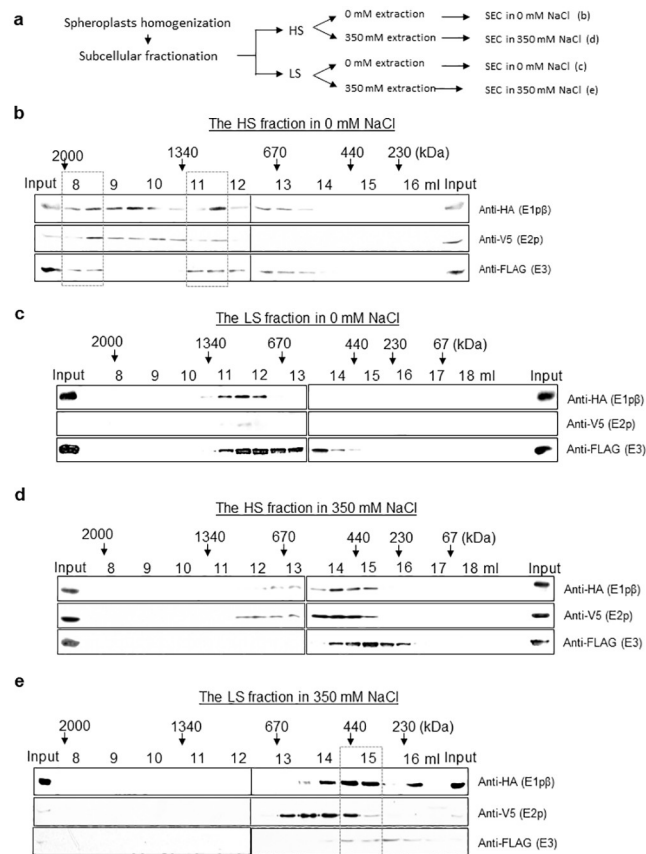


Fig 1. Ionic strength dictates the elution profiles of yPDC components in size exclusion chromatography. (a) A flowchart of experiments presented in Fig 1. For (b)-(e), size fraction profiles of yPDC components of Pdb1-3xHA/Lat1-V5/Lpd1-5xFLAG strain from (b) the HS fraction in a buffer containing 0 mM NaCl, (c) the LS fraction in a buffer containing 0 mM NaCl, (d) the HS fraction in a buffer containing 350 mM NaCl and (e) the LS fraction in a buffer containing 350 mM NaCl. Elution volumes in the SEC via Superose 6 column for every 500 μ l fraction are indicated with the expected size of eluted proteins based on standard proteins. Boxes in dashed lines highlight the peak fractions.

<https://doi.org/10.1371/journal.pone.0243489.g001>

Results

Yeast PDC components display salt-lability

We analyzed the size of the yeast PDC by size exclusion chromatography (SEC) (Fig 1a and S2a Fig in S1 File). To facilitate the detection of the PDC components, yeast BY4741 strains were generated in which combinations of the E1p β subunit (E1p β), E2p and E3 were epitope-tagged at their endogenous locus with 3xHA, V5 and 5xFLAG, respectively. We verified the epitope-tagging did not affect the growth by spotting assay of the tagged strains versus wild-type on YPD plates (S1 Fig in S1 File). When PDC E1p or E3 subunits is deleted, yeast cells become sensitive to rapamycin [39]. The PDC subunit tagged strains, however, did not display such rapamycin sensitivity compared to wildtype (S1 Fig in S1 File), thus, the epitope tags did not cause a cellular dysfunction of PDC. Next, whole-cell extracts of these strains were prepared and loaded onto a Superose 6 column for SEC. The SEC fractions were analyzed by immunoblotting using antibodies against the epitope tags on the PDC components (S2b Fig in S1 File). Interestingly, all of the three PDC components eluted at two peak fractions belonging to different sizes; one in the void volume at 8 ml (≥ 2 MDa) as expected for its well-known

macromolecular structure and the other in the range of 14–15 ml elution volume. The two clear peak elution volumes suggested a heterogeneity in the size of the PDC components, hence we decided to investigate this further.

Recent reports have demonstrated the existence of PDC in the nucleus of mammalian cells which is a non-canonical location for this mitochondrial complex [5–7]. We were curious whether the two elution peaks observed resulted from PDC that belonged to the two different subcellular organelles. To address this, we first fractionated subcellular organelles by differential sedimentation rates upon centrifugation [40]. Indeed, high sedimentation rate fraction (HS) was enriched with mitochondria, while low sedimentation rate fraction (LS) was enriched with nuclei (S2c Fig in [S1 File](#)). Each of the two enriched extracts was size-fractionated by SEC, and the fractions were collected and probed for PDC components by immunoblotting against their epitope tags ([Fig 1b and 1e](#)). From the (mitochondria-enriched) HS extract, the elution of the PDC components peaked at 8 ml for several MDa (≥ 2 MDa) as well as at 11–12 ml for ~1 MDa proteins ([Fig 1b](#)), while from the (nuclei-enriched) LS fraction, the PDC components were detected at 14–15 ml elution volume for ~230–440 kDa proteins ([Fig 1e](#)).

These results seemed to suggest that the size of the PDC differed when extracted from the different subcellular organelles at a first glance, however, the difference in ionic strength between the buffers for preparing the fractions (0 mM for HS fractions vs 350 mM for LS) may have affected the apparent size difference observed. To address this possibility, HS and LS extracts were prepared in the inversed salt conditions. Consequently, HS extract was prepared in the presence of 350 mM NaCl, whereas the LS extract was prepared in 0 mM NaCl. Then each extract was loaded onto a sizing column in the corresponding ionic strength. The eluted fractions from SEC were collected and probed for the epitope-tagged PDC components by immunoblotting ([Fig 1c and 1d](#)). All the PDC components of HS extract in 350 mM NaCl mostly eluted at 14–15 ml corresponding to molecular weight of ~230–440 kDa ([Fig 1d](#)), whereas those of LS extract in 0 mM NaCl eluted peak at 11–12 ml elution volume for ~1 MDa ([Fig 1c](#)). This result suggested that indeed the PDC of HS fraction acquired a similar SEC elution profile to that of LS fraction in the same NaCl concentration. These data suggested that the size of the PDC components can vary depending on ionic strength, rather than their source of origination.

So far, we have observed that the PDC components in low ionic strength (0 or 50 mM NaCl) eluted very differently compared to that in high ionic strength (350 mM NaCl) on a sizing column. Next, we inquired how the elution profile would behave in a physiological salt concentration of 150 mM NaCl. For this, whole-cell extract was prepared in a buffer containing 150 mM NaCl and subjected to SEC. The size-fractions were collected and immunoblotted against PDC components via their epitope tags (S2d Fig in [S1 File](#)). Interestingly, all the PDC components peaked at the elution volume of 14–15 ml for ~230–440 kDa in 150 mM NaCl. This was clearly shifted to a smaller size compared to the peak elution in the low ionic strength, at 8 ml (in 0 mM and 50 mM NaCl) and 11–12 ml elution volume (in 0 mM NaCl) ([Fig 1b and S2b Fig in S1 File](#)), suggesting the decreased size of the PDC components in the physiological salt condition. Notably, the size of the small PDC components was reminiscent of that observed in the higher ionic strength (350 mM NaCl) ([Fig 1d and 1e](#)). Further, MDa sized PDC components that were observed in lower ionic strength ([Fig 1b and S2b Fig in S1 File](#)) were substantially reduced in the ionic strength of 150 mM NaCl.

Next, to verify the ionic strength-dependent size of the PDC components irrespective of the origin of the extract, HS and LS extracts were prepared and subjected to SEC in 150 mM NaCl. The size-fractions were collected and probed for the PDC components by immunoblotting against their epitope tags (S2e–S2f Fig in [S1 File](#)). As in the SEC of whole-cell extract (S2d Fig in [S1 File](#)), the elution peaks of the PDC components in both HS and LS extracts were shifted

to a smaller size of 14–15 ml elution volume comparable to that in the high ionic strength (350 mM NaCl) buffer (Fig 1d and 1e). These results indicate that the molecular weight of the PDC components responds to changes in the ionic strength. In fact, the physiological ionic strength (150 mM NaCl) is enough to form sub-megadalton PDC components.

PDC is a salt-labile complex

Thus far, we observed that the size of the PDC components is dependent on ionic strength using SEC of various extracts (Fig 1 and S2 Fig in S1 File). To examine whether the purified complex also exhibits a similar behavior, we decided to affinity-purify PDC. For this, strains each expressing a FLAG-tagged E1p β and E3, were generated. Next, the PDC components were affinity-purified (AP) from cell extracts and the purified complexes were subjected to a mass spectrometry technique known as Multidimensional protein identification technology (MudPIT) [34]. Consistent with the fact that E1p, E2p, and E3 interact with one another in the complex, MudPIT detected all the PDC components in each of the purifications (S3a Fig in S1 File). Next, the purified complexes via E1p β -5xFLAG (Fig 2a) and E3-5xFLAG (Fig 2b) were size-fractionated in 350 mM NaCl and the fractions were probed for their elution profiles by immunoblotting against FLAG. Indeed, both purifications of PDC via E1p β and E3 showed a

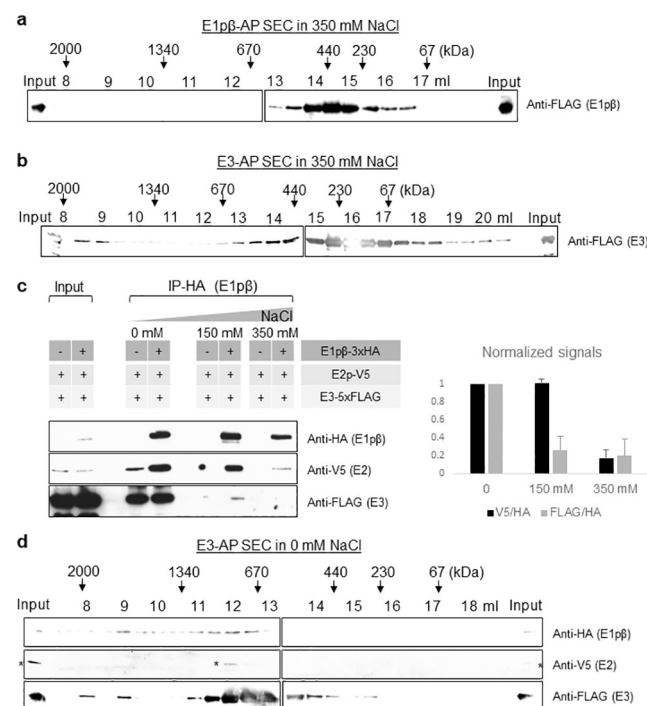


Fig 2. Affinity-purified PDC in SEC and IP suggests that yPDC is a salt-labile complex. (a) Size fraction profiles of FLAG affinity purified (AP) yPDC-E1 β from Pdb1-5xFLAG strain in a buffer containing 350 mM NaCl. (b) Size fraction profiles of FLAG purified yPDC-E3 from Lpd1-5xFLAG strain in a buffer containing 350 mM NaCl. (c) (Left panel) Immunoprecipitation (IP) of yPDC-E1 β via HA from Pdb1-3xHA/Lat1-V5/Lpd1-5xFLAG strain in a buffer containing 0 mM, 150 mM, or 350 mM of NaCl. (Right panel) The relative ratios of anti-V5 and anti-FLAG to anti-HA signals are normalized to that of 0 mM and presented with error bars indicating standard deviation of three biological replicates. (d) Size fraction profiles of FLAG AP yPDC-E3 from Pdb1-3xHA/Lat1-V5/Lpd1-5xFLAG strain in a buffer containing 0 mM NaCl. Asterisks denote non-specific signals. For (a), (b), and (d) elution volumes in the SEC via Superose 6 column for every 500 μ l fraction are indicated with the expected size of eluted proteins based on standard proteins.

<https://doi.org/10.1371/journal.pone.0243489.g002>

very similar elution profile to what we observed from the extracts in the same ionic strength (Fig 1d–1e). This result suggests that the purified PDC is as salt-labile as its components.

Since the canonical PDC contains multiple copies of E1p, E2p, and E3 subunits, we set out to determine whether the interactions among the subunits were reduced with increasing ionic strength. If so, this would explain the decreased size of the complex observed. Consequently, E1p β was immunoprecipitated (IP) via HA from whole-cell extract in varying ionic strengths and the amount of co-precipitated E2p and E3 subunits were examined by immunoblotting against their epitope tags (Fig 2c). Indeed, the amount of co-precipitated E2p and E3 decreased with increasing ionic strength, consistent with the decreased size observed by SEC. This result suggests that the PDC in higher ionic strength might contain fewer copies of one or more subunits and thereby, have a smaller size. Collectively, these results suggest that the PDC is a salt-labile complex which can dissociate in the physiological salt condition (150 mM NaCl). This contrasts with many protein complexes (e.g. SAGA, SWI/SNF, etc) that are stable in similar conditions [41].

To further validate whether the different sizes of the PDC components observed from cell extracts resulted from the varying size of the complex, we purified the PDC via E3-5xFLAG followed by SEC in 0 mM NaCl condition. The presence of the complex was detected by immunoblotting against the epitopes of the co-purified PDC components (Fig 2d). Indeed, the elution profiles of the purified PDC matched well with those obtained from extracts (Fig 1b), suggesting that the complex eluted with a higher molecular weight (≥ 2 MDa and ~ 1 MDa) in the lower ionic strength condition. Interestingly, while the E3-AP followed by SEC revealed the complex of MDa sizes (Fig 2d), it was missing the elution peak of ~ 230 kDa at 15–16 ml elution volume that was present in the SEC of E3-AP in 350 mM NaCl (Fig 2b). Similarly, the E1p β purified with the E3-AP in 0 mM NaCl (Fig 2d) did not display the peak of the SEC of E1p β -AP in 350 mM NaCl (Fig 2a) at 14–15 ml elution volume. We inquired whether the small ~ 440 kDa entity in E1p β -AP and the ~ 230 kDa entity in E3-AP observed only in the high ionic strength (350 mM NaCl) were forming a complex. To answer that, we subjected the peak sub-megadalton fraction of the SEC of each purification performed in 350 mM NaCl condition (Fig 2a and 2b) to mass spectrometry (S3b Fig in S1 File). Surprisingly, the MudPIT analysis revealed that in E1p β purification, E1p α and E1p β are the primary molecules in the co-eluting entity at the elution volume of 14.5 ml. Likewise, in the E3 purification, E3 was the main molecule at the elution volume of 16 ml. Based on the MudPIT data and previous studies [14], the peak elution volume for each PDC purification at 350 mM NaCl (Fig 2a and 2b) likely contained an oligomer of the bait subunit. Based on the elution volume, purified E1p eluted with a size of ~ 440 kDa and purified PDC-E3 eluted with a size of ~ 230 kDa.

Taken together, our data establish that the PDC is salt-labile and its integrity as a megadalton complex does not remain intact at the physiological ionic strength. Consequently, the size and the number of subunits of the complex are highly dependent on ionic strength.

Mammalian PDC also exhibits salt lability that is similar, but not identical, to that observed in yeast

PDC subunits in Baker yeast have conserved homology and sequence similarity with mammalian counterparts. Hence, we wanted to test whether the observed salt-lability of PDC is a unique property of yeast PDC (yPDC) or is conserved in the mammalian PDC (mPDC) as well. For this, HEK293T lysate was prepared and subjected to SEC in high ionic strength (350 mM). Then the size fractionated PDC components were probed by immunoblotting (Fig 3a). As in yeast, the mammalian E1p, mE1p α (PDHA1) and mE1p β (PDHB1), and mE3 components were detected mostly in sub-megadalton size fractions (~ 230 kDa) in the high ionic

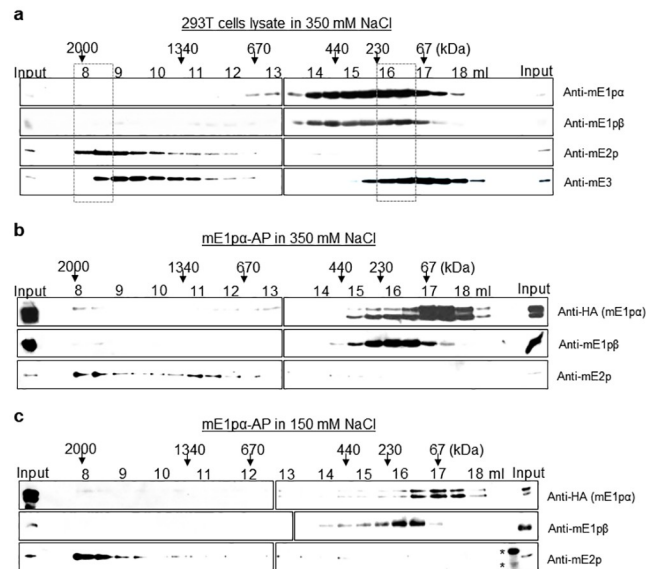


Fig 3. SEC of mammalian PDC exhibits salt-lability similar, but not identical, to that observed in yPDC. (a) Size fractionation profiles of lysates of HEK293T cells in a buffer containing 350 mM NaCl. (b) Size fractionation profiles of Halo affinity purified (AP) mE1 α construct from HEK293T cells in a buffer containing 350 mM NaCl. (c) Size fractionation profiles of affinity purified mE1 α construct from HEK293T cells in a buffer containing 150 mM NaCl. Asterisks denote non-specific signals. Elution volumes in the SEC via Superose 6 column for every 500 μ l fraction are indicated with the expected size of eluted proteins based on standard proteins. Boxes in dashed lines highlight the peak fractions.

<https://doi.org/10.1371/journal.pone.0243489.g003>

strength. Interestingly, the mE2p eluted only as a megadalton complex (≥ 2 MDa) even in the high salt condition. When the same size-fractions were probed for the subunits of a well characterized high molecular weight SWI-SNF complex, Brg1 and Baf155, by immunoblotting (S4a Fig in S1 File), they were found in megadalton size (1.3–1.5 MDa) fractions as expected. This result suggests that the mPDC components are more salt-labile than the SWI-SNF complex components (S4b Fig in S1 File).

To verify whether the co-fractionated mPDC components (Fig 3a) were forming a complex, purification of mPDC via mE1 α (PDHA1) was performed from HEK293T cells. The location of the fused protein (HaloTag) for the purification was determined based on the localization of the C-terminally YFP-tagged (PDHA1-YFP) and the N-terminally GFP-tagged (GFP-PDHA1) mE1 α (S5a Fig in S1 File). The microscopy images revealed that C-terminal tagging allowed the correct localization of the PDC component as suggested by the colocalization of PDHA1-YFP with a mitochondrial staining dye mitotracker, while the N-terminal tagging resulted in pan-cellular localization likely due to the unavailability of the mitochondrial localization sequence at the N-terminus of the precursor of the mE1 α [42].

Consequently, the mPDC was purified via PDHA1-HA-Halo construct from HEK293T cells in a buffer containing 150 mM NaCl and subjected to mass spectrometry (S5b Fig in S1 File). The MudPIT analysis identified all the subunits of mPDC, suggesting the intact complex was purified. When the purification of the presumably-mislocalized Halo-PDHA1 was subjected to mass spectrometry, MudPIT analysis (S5c Fig in S1 File) revealed that the amount of co-purified PDC subunits was significantly less as expected. Next, the mPDC purified via PDHA1-HA-Halo was subjected to SEC in high ionic strength (350 mM NaCl) and the eluted fractions were probed by immunoblotting against its components (Fig 3b). The purified mPDC essentially displayed the same profile to that acquired from the cell lysate (Fig 3a). The purified mE1 α , mE1 β and mE2p (Fig 3b) were eluted at 8–9 ml and 16–17 ml elution

volume which matched well with those in the SEC of cell lysate (Fig 3a). mE1p α and mE1p β were mostly co-eluted at fractions for a sub-megadalton (~ 230 kDa) protein, likely as mE1p α 2 β 2 tetramers in this high ionic strength condition. With an elution peak at the void volume, the mE2p seemed to only co-elute with a complex of several megadaltons (≥ 2 MDa) in size. These results suggest that mE1p is salt-labile while mE2p core is stable in high ionic strength.

Next, we inquired how the mPDC would behave in the physiological condition at 150 mM NaCl. To address that, the mPDC was purified via PDHA1-HA-Halo from HEK293T cells in a buffer containing 150 mM NaCl and subjected to SEC. The size-fractions in 150 mM NaCl were collected and probed for the mPDC components by immunoblotting (Fig 3c). As observed with the yPDC, the mPDC displayed a similar elution profile in this physiological condition as it did with the high ionic strength (350 mM NaCl) (Fig 3b). The mE1p α and mE1p β co-eluted in a sub-megadalton entity of ~230 kDa, while the mE2p eluted at 8–9 ml elution volume with a complex of several megadaltons. The mPDC exhibited a striking difference as compared to yPDC in that the mE2p was more stable as a megadalton complex in high ionic strength. However, mE1p also exhibited a sub-megadalton size in a physiological condition like yE1p. The mE3 in the mE1p α -AP was below detection level in western blots (not shown). Next, the mPDC was purified via PDHA1-HA-Halo from HEK293T cells in low ionic strength (0 mM NaCl). Both mE1p α and mE2p displayed SEC elution profile with increased amount of MDa sizes compared to that in 350 mM and 150 mM condition (S6 Fig in S1 File). These results suggest that the salt-lability is conserved from yeast to human and might be a universal property of E1p, while the lability of E2p may differ between organisms.

The catalytic activity of PDC changes with ionic strength

Thus far, we have established that the PDC is a salt-labile complex compared to other protein complexes such as the SWI/SNF which maintains its integrity in high salt conditions (S4 Fig in S1 File). This finding led us to speculate whether the salt lability of the complex affects its activity. Previously, a non-canonically smaller PDC observed in the process of reassembling or disassembling canonical PDC showed lower catalytic activity proportional to its size [43, 44]. Thus, we postulated that ionic strength, with which the size of the PDC can vary, can modulate the activity of the PDC. To test this hypothesis, we performed *in vitro* catalytic activity assay of the PDC. The yPDC was affinity-purified in a low salt condition (50 mM NaCl) from a PDC kinase mutant via E1p β (*pkp2 Δ /PDB1-5xFLAG*) to account for the highly phosphorylated inactive PDC in yeast [45]. To examine the effect of ionic strength on the PDC activity, the assay was performed with a low (50 mM NaCl) and a high (350 mM) ionic strength.

Iodonitrotetrazolium chloride (INT)-salt adduct produced by the catalytic activity of PDC was detected by absorbance at 490 nm over a time course (see [Material and method](#) for details). Indeed, a lower activity was detected in the PDC in higher ionic strength (350 mM NaCl) compared to that in lower ionic strength (50 mM NaCl) (Fig 4a). In the control experiment in which the PDC was removed from the assay, the absorbance at 490 nm remained constant in both ionic strength conditions. The amount of PDC used in the two assays was verified to be equivalent by immunoblotting of the E1p β -FLAG (S7 Fig in S1 File).

Next, to corroborate that it was the ionic strength imposed on the PDC that led to the change in the activity, we performed the assay in two conditions with a single ionic strength (100 mM NaCl), while the PDC was pre-incubated in a low (50 mM NaCl) or a high (350 mM NaCl) ionic strength condition prior to the assay (Fig 4b). Indeed, the decrease in the activity was observed when the PDC was exposed to a higher ionic strength prior to the assay. This suggested that the high ionic strength decreased the activity of PDC. Taken together, these

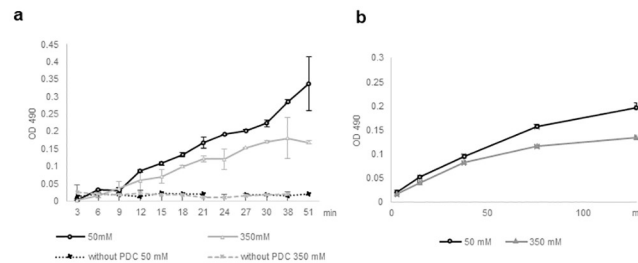


Fig 4. The labile character of PDC is correlated with catalytic activity. The catalytic activity of yPDC measured by absorbance at 490 nm via INT in the presence of (a) 0.6 mM INT and 50 mM or 350 mM NaCl or (b) 0.4 mM INT and 100 mM NaCl with yPDC preincubated with 50 mM or 350 mM NaCl. Error bars indicate standard deviations of three replicates.

<https://doi.org/10.1371/journal.pone.0243489.g004>

results suggest that the ionic strength that affects the size of PDC can modulate its catalytic activity possibly by changing the number of subunits within the complex.

Discussion

The present study demonstrates the lability of the multienzyme PDC. Several reports have shown that the PDC size, structure, and the number of its subunits can vary up to ~17% [29, 30, 46–49]. However, the present study is the first report that in a systematic way establishes the lability of the PDC that forms sub-megadalton structure in the physiological ionic strength.

The E1p is known to form a tetramer (E1 α 2 β 2), which is calculated to be ~180 kDa, within the yPDC. Interestingly, the yE1p we purified eluted at fractions for ~440 kDa proteins (Fig 2a) that mainly contained E1 α , E1 β , and a nominal amount of E2p (S3b Fig in S1 File). PDC kinases and phosphatases have been shown to be associated with PDC by binding to E2p, but the regulatory proteins were not detected in our affinity purifications [50]. This suggests the possibility of a larger oligomer of yE1p. The E3 is known to form a homodimer, which is calculated to be ~120 kDa. In our affinity purification, yE3 eluted at fractions for ~230 kDa, which contained mostly E3 (S3b Fig in S1 File). This suggests a possible stable form of E3 as a tetramer as well as a dimer. These possible variations of oligomeric states of the PDC components further support our observation about the lability of the complex. The key conclusions of this study are illustrated in the model (Fig 5).

Forming a massive complex can provide cells a concentrated catalytic potential with high efficiency via substrate channeling and active-site coupling [14]. This notion is supported by a

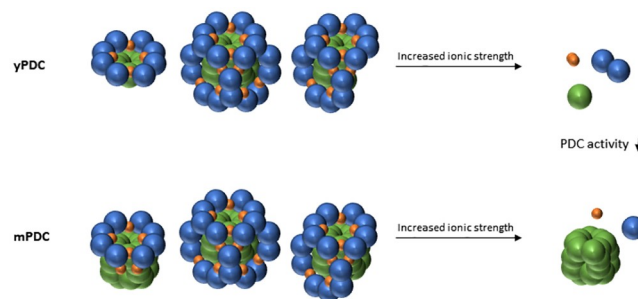


Fig 5. A model of labile PDC in yeast and human. The yeast PDC (yPDC) and the human PDC (mPDC) forming various structures dissociate in high ionic strength condition. The blue sphere represents E1 α 2 β 2, the green sphere represents E2p, and the orange sphere represents E3 dimer. E3BP is omitted for simplicity.

<https://doi.org/10.1371/journal.pone.0243489.g005>

reassembled PDC with ~42–48 E1p heterotetramers and 6–12 E3 homodimers optimally filling 60 sites of E2p core exhibiting the maximal activity of the complex [51]. However, the lability of the PDC suggests that PDC may form structures with variable sizes that can occur spontaneously. Each of the structures may be associated with a certain level of catalytic activity. Interestingly, we show that the catalytic activity of the PDC decreases with an increased ionic strength. This might be because higher ionic strength would allow fewer E1p, E2p, and/or E3 subunits in the complex leading to fewer active-site couplings, hence resulting in a less efficiency or reduced activity [15, 16]. Consistent with this, pathogenic PDC variants have been found associated with structural changes of PDC [52, 53]. The decreased activity of the PDC in such patients suggests the association of the complex structure with the activity of the complex [22]. E1p and E3 components can bind independently and competitively to the structural core formed by the E2p oligomers with different interaction property: binding of E1p is enthalpy-driven, while that of E3 is entropy-driven [20]. The varying number of E1p and E3 components can also lead to a change in the overall activity of the complex as E1p catalyzes the rate-limiting step of the overall catalysis. In fact, various combinations of the number of E1p and E3 subunits in PDC have been reported [48]. Collectively, the size and the number of component versatility of the PDC could be a means to modulate its activity. Taken together, the versatile structure of the PDC may provide a dynamic mechanism to modulate its catalytic activity.

Recent studies reported that PDC in some mammalian cells is found in the nucleus under circumstances such as in cancer and during zygotic activation in embryonic cells, potentially as a whole ~10 MDa complex [5, 6]. However, it is indecipherable how a massive protein complex with a ~450 Å size could translocate from one subcellular organelle to another even when considering the possible trafficking pathway via mitochondrial-derived vesicles (MDV) of ~100 Å in size [54]. Interestingly, a rather pliable structure that can change the size of the complex provides a means to translocate the otherwise massive protein complex. Perhaps, a smaller non-conventional sized PDC complex can translocate into the nucleus.

Supporting information

S1 File.

(PDF)

S1 Raw images.

(PDF)

S1 Data. Copy of 100mM reaction in 50mM or 350mM.

(XLSX)

S2 Data. Copy of PDC activity 490nm.

(XLSX)

S3 Data. Normalizing IP 150 mM 350 mM for Fig 2c.

(XLSX)

Acknowledgments

We thank Workman Lab members and Stowers core facilities for their support during this work.

Author Contributions

Conceptualization: Jaehyoun Lee, Jerry L. Workman.

Data curation: Jaehyoun Lee, Laurence Florens.

Formal analysis: Jaehyoun Lee.

Funding acquisition: Jerry L. Workman.

Investigation: Jaehyoun Lee, Jerry L. Workman.

Methodology: Jaehyoun Lee, Seunghee Oh, Saikat Bhattacharya, Ying Zhang, Laurence Florens, Michael P. Washburn.

Project administration: Jerry L. Workman.

Resources: Michael P. Washburn.

Supervision: Jerry L. Workman.

Validation: Jaehyoun Lee.

Visualization: Jaehyoun Lee, Saikat Bhattacharya, Ying Zhang.

Writing – original draft: Jaehyoun Lee, Jerry L. Workman.

Writing – review & editing: Seunghee Oh, Saikat Bhattacharya, Laurence Florens.

References

1. Patel KP, O'Brien TW, Subramony SH, Shuster J, Stacpoole PW. The spectrum of pyruvate dehydrogenase complex deficiency: Clinical, biochemical and genetic features in 371 patients. *Molecular Genetics and Metabolism*. 2012. pp. 385–394. <https://doi.org/10.1016/j.ymgme.2012.03.017> PMID: 22896851
2. Brunette MG, Delvin E, Hazel B, Scriver CR. Thiamine-responsive lactic acidosis in a patient with deficient low-KM pyruvate carboxylase activity in liver. *Pediatrics*. 1972; 50: 702–711. PMID: 4343503
3. Zhou Y, Zhang S, He H, Jiang W, Hou L, Xie D, et al. Design and synthesis of highly selective pyruvate dehydrogenase complex E1 inhibitors as bactericides. *Bioorganic Med Chem*. 2018; 26: 84–95. <https://doi.org/10.1016/j.bmc.2017.11.021> PMID: 29170025
4. Saunier E, Benelli C, Bortoli S. The pyruvate dehydrogenase complex in cancer: An old metabolic gatekeeper regulated by new pathways and pharmacological agents. *Int J Cancer*. 2016; 138: 809–817. <https://doi.org/10.1002/ijc.29564> PMID: 25868605
5. Sutendra G, Kinnaird A, Dromparis P, Paulin R, Stenson TH, Haromy A, et al. A nuclear pyruvate dehydrogenase complex is important for the generation of Acetyl-CoA and histone acetylation. *Cell*. 2014; 158: 84–97. <https://doi.org/10.1016/j.cell.2014.04.046> PMID: 24995980
6. Nagaraj R, Sharpley MS, Chi F, Braas D, Zhou Y, Kim R, et al. Nuclear Localization of Mitochondrial TCA Cycle Enzymes as a Critical Step in Mammalian Zygotic Genome Activation. *Cell*. 2017; 168: 210–223.e11. <https://doi.org/10.1016/j.cell.2016.12.026> PMID: 28086092
7. Chueh FY, Leong KF, Cronk RJ, Venkitachalam S, Pabich S, Yu CL. Nuclear localization of pyruvate dehydrogenase complex-E2 (PDC-E2), a mitochondrial enzyme, and its role in signal transducer and activator of transcription 5 (STAT5)-dependent gene transcription. *Cell Signal*. 2011; 23: 1170–1178. <https://doi.org/10.1016/j.cellsig.2011.03.004> PMID: 21397011
8. Matsuda S, Adachi J, Ihara M, Tanuma N, Shima H, Kakizuka A, et al. Nuclear pyruvate kinase M2 complex serves as a transcriptional coactivator of arylhydrocarbon receptor. *Nucleic Acids Res*. 2016; 44: 636–647. <https://doi.org/10.1093/nar/gkv967> PMID: 26405201
9. Patel MS, Korotchkina LG. The biochemistry of the pyruvate dehydrogenase complex. *Biochem Mol Biol Educ*. 2003; 31: 5–15. <https://doi.org/10.1002/bmb.2003.494031010156>
10. Da Silva LA, De Marcucci OL, Kuhnle ZR. Dietary polyunsaturated fats suppress the high-sucrose-induced increase of rat liver pyruvate dehydrogenase levels. *Biochim Biophys Acta (BBA)-Lipids Lipid Metab*. 1993; 1169: 126–134. [https://doi.org/10.1016/0005-2760\(93\)90197-h](https://doi.org/10.1016/0005-2760(93)90197-h) PMID: 8343536
11. Kaplon J, Zheng L, Meissl K, Chaneton B, Selivanov VA, MacKay G, et al. A key role for mitochondrial gatekeeper pyruvate dehydrogenase in oncogene-induced senescence. *Nature*. 2013; 498: 109–112. <https://doi.org/10.1038/nature12154> PMID: 23685455
12. Tso SC, Qi X, Gui WJ, Wu CY, Chuang JL, Wernstedt-Asterholm I, et al. Structure-guided development of specific pyruvate dehydrogenase kinase inhibitors targeting the ATP-binding pocket. *J Biol Chem*. 2014; 289: 4432–4443. <https://doi.org/10.1074/jbc.M113.533885> PMID: 24356970

13. Patel MS, Nemeria NS, Furey W, Jordan F. The pyruvate dehydrogenase complexes: Structure-based function and regulation. *J Biol Chem.* 2014; 289: 16615–16623. <https://doi.org/10.1074/jbc.R114.563148> PMID: 24798336
14. Reed LJ. Multienzyme complexes. *Acc Chem Res.* 1974; 7: 40–46. <https://doi.org/10.1021/ar50074a002>
15. Perham RN. Domains, Motifs, and Linkers in 2-Oxo Acid Dehydrogenase Multienzyme Complexes: A Paradigm in the Design of a Multifunctional Protein. *Biochemistry.* 1991; 30: 8501–8512. <https://doi.org/10.1021/bi00099a001> PMID: 1888719
16. Stepp LR, Bleile DM, McRorie DK, Pettit FH, Reed LJ. Use of Trypsin and Lipoamidase To Study the Role of Lipoic Acid Moieties in the Pyruvate and α -Ketoglutarate Dehydrogenase Complexes of *Escherichia coli*. *Biochemistry.* 1981; 20: 4555–4560. <https://doi.org/10.1021/bi00519a007> PMID: 6794598
17. Hackert ML, Oliver RM, Reed LJ. Evidence for a multiple random coupling mechanism in the α -ketoglutarate dehydrogenase multienzyme complex of *Escherichia coli*: A computer model analysis. 1983; 80: 2226–2230.
18. Stoops JK, Baker TS, Schroeter JP, Kolodziej SJ, Da Niu X, Reed LJ. Three-dimensional structure of the truncated core of the *Saccharomyces cerevisiae* pyruvate dehydrogenase complex determined from negative stain and cryoelectron microscopy images. *J Biol Chem.* 1992; 267: 24769–24775. PMID: 1280269
19. Milne JLS, Wu X, Borgnia MJ, Lengyel JS, Brooks BR, Shi D, et al. Molecular structure of a 9-MDa icosahedral pyruvate dehydrogenase subcomplex containing the E2 and E3 enzymes using cryoelectron microscopy. *J Biol Chem.* 2006; 281: 4364–4370. <https://doi.org/10.1074/jbc.M504363200> PMID: 16308322
20. Jung H-I, Bowden SJ, Cooper A, Perham RN. Thermodynamic analysis of the binding of component enzymes in the assembly of the pyruvate dehydrogenase multienzyme complex of *Bacillus stearothermophilus*. *Protein Sci.* 2002; 11: 1091–1100. <https://doi.org/10.1110/ps.4970102> PMID: 11967366
21. Vijayakrishnan S, Kelly SM, Gilbert RJC, Callow P, Bhella D, Forsyth T, et al. Solution structure and characterisation of the human pyruvate dehydrogenase complex core assembly. *J Mol Biol.* 2010; 399: 71–93. <https://doi.org/10.1016/j.jmb.2010.03.043> PMID: 20361979
22. Smolle M, Prior AE, Brown AE, Cooper A, Byron O, Lindsay JG. A new level of architectural complexity in the human pyruvate dehydrogenase complex. *J Biol Chem.* 2006; 281: 19772–19780. <https://doi.org/10.1074/jbc.M601140200> PMID: 16679318
23. Frank RAW, Pratap JV, Pei XY, Perham RN, Luisi BF. The molecular origins of specificity in the assembly of a multienzyme complex. *Structure.* 2005; 13: 1119–1130. <https://doi.org/10.1016/j.str.2005.04.021> PMID: 16084384
24. Brautigam CA, Wynn RM, Chuang JL, Chuang DT. Subunit and catalytic component stoichiometries of an in vitro reconstituted human pyruvate dehydrogenase complex. *J Biol Chem.* 2009; 284: 13086–13098. <https://doi.org/10.1074/jbc.M806563200> PMID: 19240034
25. Bates DL, Harrison RA, Perham RN. The stoichiometry of polypeptide chains in the pyruvate dehydrogenase multienzyme complex of *E. Coli* determined by a simple novel method. *FEBS Lett.* 1975; 60: 427–430. [https://doi.org/10.1016/0014-5793\(75\)80764-2](https://doi.org/10.1016/0014-5793(75)80764-2) PMID: 776681
26. Kok De, Arie, Westphal AH. Hybrid pyruvate dehydrogenase complexes reconstituted from components of the complexes from *Escherichia coli* and *Azotobacter vinelandii*. *FEBS Lett.* 1985; 152: 35–41. <https://doi.org/10.1111/j.1432-1033.1985.tb09160.x>
27. Danson MJ, Hale G, Johnson P, Perham RN, Smith J, Spragg P. Molecular weight and symmetry of the pyruvate dehydrogenase multienzyme complex of *Escherichia coli*. *J Mol Biol.* 1979; 129: 603–617. [https://doi.org/10.1016/0022-2836\(79\)90471-6](https://doi.org/10.1016/0022-2836(79)90471-6) PMID: 383998
28. Schmitt B, Cohen R. The structure of the *Escherichia coli* pyruvate dehydrogenase complex is probably not unique. *Biochem Biophys Res Commun.* 1980; 93: 709–712. [https://doi.org/10.1016/0006-291x\(80\)91135-3](https://doi.org/10.1016/0006-291x(80)91135-3) PMID: 6992775
29. Gilbert GA, Gilbert LM. Detection in the ultracentrifuge of protein heterogeneity by computer modelling, illustrated by pyruvate dehydrogenase multienzyme complex. *J Mol Biol.* 1980; 144: 405–408. [https://doi.org/10.1016/0022-2836\(80\)90099-6](https://doi.org/10.1016/0022-2836(80)90099-6) PMID: 7253023
30. Sumegi B, Liposits Z, Inman L, Paull WK, Srere PA. Electron microscopic study on the size of pyruvate dehydrogenase complex in situ. *Eur J Biochem.* 1987; 169: 223–230. <https://doi.org/10.1111/j.1432-1033.1987.tb13601.x> PMID: 3315661
31. Kirkwood KJ, Ahmad Y, Larance M, Lamond AI. Characterization of native protein complexes and protein isoform variation using sizefractionation-based quantitative proteomics. *Mol Cell Proteomics.* 2013; 12: 3851–3873. <https://doi.org/10.1074/mcp.M113.032367> PMID: 24043423

32. Suganuma T, Gutiérrez JL, Li B, Florens L, Swanson SK, Washburn MP, et al. ATAC is a double histone acetyltransferase complex that stimulates nucleosome sliding. *Nat Struct Mol Biol.* 2008; 15: 364–372. <https://doi.org/10.1038/nsmb.1397> PMID: 18327268
33. Hinman LM, Blass JP. An NADH-linked spectrophotometric assay for pyruvate dehydrogenase complex in crude tissue homogenates. *J Biol Chem.* 1981; 256: 6583–6586. PMID: 7240230
34. Florens L, Washburn MP. Proteomic analysis by multidimensional protein identification technology. *Methods Mol Biol.* 2006; 328: 159–175. <https://doi.org/10.1385/1-59745-026-X:159> PMID: 16785648
35. Zhang Y, Wen Z, Washburn MP, Florens L. Improving proteomics mass accuracy by dynamic offline lock mass. *Anal Chem.* 2011; 83: 9344–9351. <https://doi.org/10.1021/ac201867h> PMID: 22044264
36. Xu T, Park SK, Venable JD, Wohlschlegel JA, Diedrich JK, Cociorva D, et al. ProLuCID: An improved SEQUEST-like algorithm with enhanced sensitivity and specificity. *J Proteomics.* 2015; 129: 16–24. <https://doi.org/10.1016/j.jprot.2015.07.001> PMID: 26171723
37. Tabb DL, McDonald WH, Yates JR. DTASelect and contrast: Tools for assembling and comparing protein identifications from shotgun proteomics. *J Proteome Res.* 2002; 1: 21–26. <https://doi.org/10.1021/pr015504q> PMID: 12643522
38. Zhang Y, Wen Z, Washburn MP, Florens L. Refinements to label free proteome quantitation: How to deal with peptides shared by multiple proteins. *Anal Chem.* 2010; 82: 2272–2281. <https://doi.org/10.1021/ac9023999> PMID: 20166708
39. Kingsbury JM, Sen ND, Cardenas ME. Branched-Chain Aminotransferases Control TORC1 Signaling in *Saccharomyces cerevisiae*. *PLoS Genet.* 2015; 11: 1–24. <https://doi.org/10.1371/journal.pgen.1005714> PMID: 26659116
40. Gregg C, Kyryakov P, Titorenko VI. Purification of mitochondria from yeast cells. *J Vis Exp.* 2009. <https://doi.org/10.3791/1417> PMID: 19704406
41. Prochasson P, Neely KE, Hassan AH, Li B, Workman JL. Targeting activity is required for SWI/SNF function in vivo and is accomplished through two partially redundant activator-interaction domains. *Mol Cell.* 2003; 12: 983–990. [https://doi.org/10.1016/s1097-2765\(03\)00366-6](https://doi.org/10.1016/s1097-2765(03)00366-6) PMID: 14580348
42. de Boer VCJ, Houten SM. A mitochondrial expatriate: Nuclear pyruvate dehydrogenase. *Cell.* 2014; 158: 9–10. <https://doi.org/10.1016/j.cell.2014.06.018> PMID: 24995972
43. Bates DL, Danson MJ, Hale G, Hooper EA, Perham RN. Self-assembly and catalytic activity of the pyruvate dehydrogenase multienzyme complex of *Escherichia coli*. *Nature.* 1977; 268: 313–316. <https://doi.org/10.1038/268313a0> PMID: 329143
44. Schwartz ER, Reed LJ. Alpha-keto acid dehydrogenase complexes. XII. Effects of acetylation on the activity and structure of the dihydrolipoyl transacetylase of *Escherichia coli*. *J Biol Chem.* 1969; 244: 6074–6079. PMID: 4900507
45. Gey U, Czupalla C, Hofflack B, Rödel G, Krause-Buchholz U. Yeast pyruvate dehydrogenase complex is regulated by a concerted activity of two kinases and two phosphatases. *J Biol Chem.* 2008; 283: 9759–9767. <https://doi.org/10.1074/jbc.M708779200> PMID: 18180296
46. Gu Y, Zhou ZH, McCarthy DB, Reed LJ, Stoops JK. 3D electron microscopy reveals the variable deposition and protein dynamics of the peripheral pyruvate dehydrogenase component about the core. *Proc Natl Acad Sci U S A.* 2003; 100: 7015–7020. <https://doi.org/10.1073/pnas.0732060100> PMID: 12756305
47. Pawelczyk T, Olson MS. Changes in the structure of pyruvate dehydrogenase complex induced by mono- and divalent ions. *Int J Biochem Cell Biol.* 1995; 27: 513–521. [https://doi.org/10.1016/1357-2725\(95\)00006-b](https://doi.org/10.1016/1357-2725(95)00006-b) PMID: 7641081
48. Oliver RM, Reed LJ. in *Electron Microscopy of Proteins*. Academic Press, London. 1982.
49. Stoops JK, Cheng RH, Yazdi MA, Maeng CY, Schroeter JP, Klueppelberg U, et al. On the unique structural organization of the *Saccharomyces cerevisiae* pyruvate dehydrogenase complex. *J Biol Chem.* 1997; 272: 5757–5764. <https://doi.org/10.1074/jbc.272.9.5757> PMID: 9038189
50. Harris RA, Bowker-Kinley MM, Huang B, Wu P. Regulation of the activity of the pyruvate dehydrogenase complex. *Advances in Enzyme Regulation.* 2002. pp. 249–259. [https://doi.org/10.1016/s0065-2571\(01\)00061-9](https://doi.org/10.1016/s0065-2571(01)00061-9) PMID: 12123719
51. Perham RN. Swinging Arms and Swinging Domains in Multifunctional Enzymes: Catalytic Machines for Multistep Reactions. *Annu Rev Biochem.* 2000; 69: 961–1004. <https://doi.org/10.1146/annurev.biochem.69.1.961> PMID: 10966480
52. Ling M, McEachern G, Seyda A, MacKay N, Scherer SW, Bratinova S, et al. Detection of a homozygous four base pair deletion in the protein X gene in a case of pyruvate dehydrogenase complex deficiency. *Hum Mol Genet.* 1998; 7: 501–505. <https://doi.org/10.1093/hmg/7.3.501> PMID: 9467010

53. Drakulic S, Rai J, Vang S, Monika P, Sander B. Folding and assembly defects of pyruvate dehydrogenase deficiency—related variants in the E1 α subunit of the pyruvate dehydrogenase complex. *Cell Mol Life Sci.* 2018; 75: 3009–3026. <https://doi.org/10.1007/s00018-018-2775-2> PMID: 29445841
54. Ng F, Tang BL. Pyruvate dehydrogenase complex (PDC) export from the mitochondrial matrix. *Mol Membr Biol.* 2014; 31: 207–210. <https://doi.org/10.3109/09687688.2014.987183> PMID: 25495576